

Cell viability of fine powders in hybrid resins and ceramic materials for CAD/CAM

Mariko NAKAI¹, Koichi IMAI^{2,3} and Yoshiya HASHIMOTO¹

¹ Department of Biomaterials, Faculty of Dentistry, Osaka Dental University, 8-1 Kuzuhahanazono-cho, Hirakata, Osaka 573-1121, Japan

² Department of Tissue Engineering, Faculty of Dentistry, Osaka Dental University, 8-1 Kuzuhahanazono-cho, Hirakata, Osaka 573-1121, Japan

³ Graduate School of Health Sciences, Osaka Dental University, 1-4-4 Makinohon-cho, Hirakata, Osaka, 573-1144, Japan

Corresponding author, Mariko NAKAI; E-mail: nakai-m@cc.osaka-dent.ac.jp

Resin blocks and ceramic blocks for CAD/CAM crowns were cut into powders and separated into three particle size groups. Oxidative stress and cell viability were measured in 3T3 and FRSK cells. The results of cytotoxicity tended to be slightly higher for resin than for ceramics. The values also increased as the particle size decreased in the powders. In addition, incorporation into cells was frequently observed under SEM, suggesting that the particle size of easily incorporated dust is different among cell types. Fluorescence-activated cell sorter (FACS) showed an increase in apoptosis and a decrease in cell viability in most of the sample groups compared to the control group. Hematoxylin and eosin staining of the cells showed deep staining of the nuclei in the sample groups. It was found that oxidative stress cell viability and apoptosis appeared differently depending on the size of the particles and the type of cells.

Keywords: CAD/CAM, Composite resin blocks ceramic blocks, Cell viability

INTRODUCTION

The use of resin and ceramic materials for CAD/CAM crowns has rapidly increased in Japan due to an increase in esthetic demand from patients, in metal prices, and in metal-free repair to deal with metal allergy¹. The resistance to wear and discoloration of resin materials for CAD/CAM crowns are excellent compared with those of conventional dental composite resins since prostheses using these are prepared by cutting a hardening body with a high rate of polymerization. In addition, UDMA and TEGDMA are used for the resin matrix in many cases, so that almost no unpolymerized layer is present and the structure is a 3-dimensional network structure, leading to excellent strength². On the other hand, ceramic materials have color and transparency similar to those of natural teeth and are superior in hardness, wear resistance, chemical stability, and biocompatibility. Discoloration is also small; however, the impact resistance is slightly inferior. Ceramic materials are classified into those using silica and those using aluminum and zirconium as the principal ingredient³.

Physical evaluation of block materials for CAD/CAM has been frequently performed⁴⁻⁷. Adjustment by a dentist is necessary for attachment of CAD/CAM crowns in approximately 20% of cases^{8,9}. Fine powders containing nano- or submicron-sized particles may be produced during grinding and cutting. The production of dust during dental practice and grinding dental materials, in addition to those for CAD/CAM crowns has been considered problematic¹⁰⁻¹². The influence of inhalation and adhesion to the body surface of dust is of

concern^{13,14}. Moreover, the repair material may wear with time in the oral cavity after prosthesis attachment^{15,16}. The presence of microparticles released from a nano-filler-containing dental crown repair material due to wear of the material has been reported in literature¹⁷.

There are various methods for biological safety evaluation of dental materials, and they are specified by the international standards ISO 1993, ISO 7405, and JIS T 6001. Regarding cytotoxicity tests, there are various experimental methods for *in vitro* testing. Biosafety tests of materials for CAD/CAM, such as the direct contact test and extraction test, are performed using a block, and it has been reported that both resin and ceramic materials may have almost no or only a slight influence on cells in the conventional cytotoxicity test¹⁸⁻²⁰. In addition to focusing on the effects on epithelial cells in the case of adhesion to the body surface, it is also necessary to consider the effects on connective tissues. This is because fine particles may enter connective tissues when adhering to wounded skin or mucous membranes. However, there have been no reports on these in a form other than block, such as fine powder. A difference in cytotoxicity in nano- and submicron samples compared with that observed in the conventional cytotoxicity test has been reported in the past^{21,22}. Furthermore, differences in cytotoxicity due to differences in particle shape and among the cell types tested have been reported²³⁻²⁶. The oral cavity tissue is composed of mesoderm-derived connective tissue and ectoderm-derived epithelial tissue, suggesting that the result may be different between connective tissue cells and epithelial cells, even though the material is the same.

We tried evaluation using 2 types of rodent-derived

Color figures can be viewed in the online issue, which is available at J-STAGE.

Received Sep 23, 2021; Accepted Jan 5, 2022

doi:10.4012/dmj.2021-261 JOI JST.JSTAGE/dmj/2021-261

cells. Fine powders of resin and ceramic materials for CAD/CAM crowns were prepared by cutting and were exposed to the two types of cells. Phagocytosis by the cells was observed, and the influence of the particle size of fine powder on oxidative stress, cell viability, and apoptosis was investigated accordingly.

MATERIALS AND METHODS

Materials

Three types of resin blocks and two types of ceramic blocks for CAD/CAM crowns generally sold in Japan were used in this study (Table 1).

Preparation and analysis of powder samples

An autoclaved diamond disc for dental (Diamantscheibe Ultraflex, NTI-Kahla, Kahla, Germany) purpose was attached to a micro motor handpiece, and each block fixed to the sample table was cut into powder. The powder was collected on sterilized aluminum foil, washed sufficiently, and sterilized with EOG gas.

Since the composition of the contained monomer and detailed information on the content of the three types of resin material were not disclosed, whether there was a large difference among the three types was analyzed using Fourier transform infrared spectroscopy (FT-IR; IRAffinity-1S, Shimadzu, Kyoto, Japan) and the quest single reflection ATR accessory (Shimadzu). In addition, powder samples were observed using a scanning electron microscope (SEM; S-4800, Hitachi High-Tech, Tokyo, Japan). The particles in the field of view were counted repeatedly, and 420–500 particles were finally recorded. Furthermore, the particle size distribution was determined from the SEM images using the image analysis software Image J (National Institutes of Health, Bethesda, MA, USA).

Cell culture

Mouse-derived fibroblast-like cells, Balb/c 3T3 cells (Fig. 1a), and fetal rat skin-derived keratinocytes, FRSK cells (Fig. 1b), were used in this study. 3T3 cells were obtained from the Riken BioResource Research Center (Ibaraki, Japan), and FRSK cells were obtained from

JCRB cell bank (Osaka, Japan). D-MEM (FUJIFILM Wako Pure Chemical, Osaka, Japan) supplemented with fetal bovine serum Hyclone™ (USDA Tested, processed in USA, lot. AD16384277, Cytiva, Tokyo, Japan) was used at a volume ratio of 10%.

Preparation of test solutions and exposure of cells

Each powder sample was added to the assay medium at a concentration of 1 mg/mL. After strong stirring using

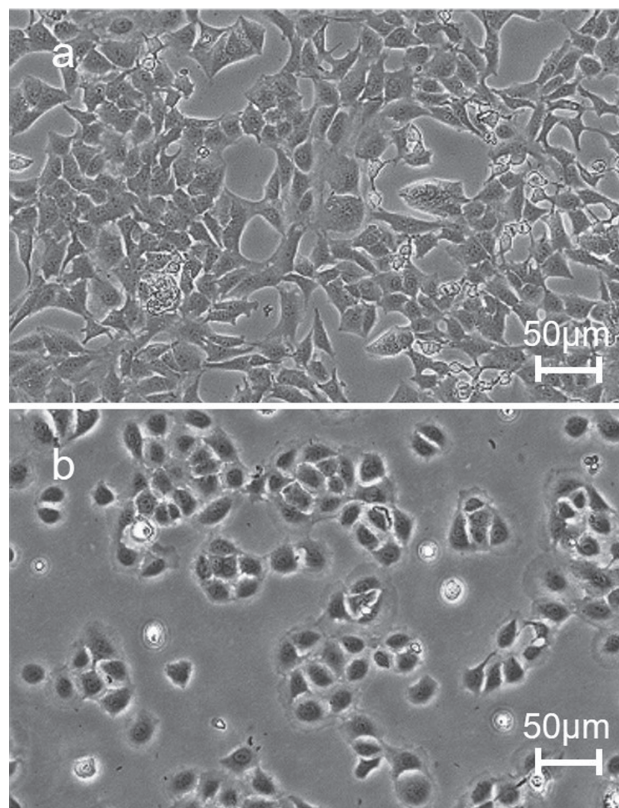


Fig. 1 Inverted phase contrast microscopy image of each cell cultured in DMEM supplemented with 10% FBS.

a: Balb c/3T3 cells, b: FRSK cells

Table 1 Materials used

Brand	Manufacturers	Code	Shade	Lot.No
KATANA® AVENCIA® Block*	Kuraray Noritake Dental, Tokyo, Japan	KA	A2	000421
SHOFU Block HC*	Shofu, Kyoto, Japan	SB	A2	0419687
ARTESANO*	Yamahachi Dental MFG, Aichi, Japan	AR	A2	0A10
VITABLOCS® MarkII**	VITA Zahnfabrik, Bad Sackingen, Germany	VM	A2C	78360
IPS Empress® CAD**	Ivoclar Vivadent, Tokyo, Japan	IE	A2	K02605

*Hybrid resin **Ceramic

a desk-top vibrator, the powder was separated into three particle size groups (40 μm or larger, 5–40 μm , and 5 μm or smaller) using two types of cell strainers (40 and 5 μm), and a total of 15 test solutions were thus prepared. The numbers of 3T3 and FRSK cells were adjusted to 1.0×10^5 cells/mL using a disposable hemocytometer, and the cells were aliquoted at 100 μL /well in a 96-well-multiplate (AGC TECHNO GLASS, Shizuoka, Japan) using a multi-pipet and were subjected to static culture for 24 h in a CO_2 incubator (37°C, 5% CO_2 , 95% air). After confirming the normal extension of each cell on the bottom surface of the well under an inverted phase-contrast microscope (Olympus, Tokyo, Japan), the culture fluid was exchanged with 100 μL /well of each test solution, followed by 3-day static culturing in the CO_2 incubator as described above. For the control group, an assay medium containing no sample was added accordingly.

Evaluation

1. Measurement of oxidative stress by ROS

Since peroxides and free radicals are produced in cells due to oxidative stress by reactive oxygen species, damaged proteins, lipids, and DNA, thus impairing organelles, oxidative stress was evaluated by ROS assay. The number of cells was adjusted to 1.0×10^5 cells/mL, and each cell type was seeded in a 96-well-multiplate and subjected to 24 h static culture in a CO_2 incubator. The culture fluid was exchanged with 100 μL /well of each test solution. After 6 h of culture, the test solution was discarded, each well was washed with DMEM, and a highly sensitive DCFH-DA working solution of ROS Assay Kit (Dojindo Laboratories, Kumamoto, Japan) was aliquoted at 100 μL /well, followed by incubation for 30 min. After the supernatant was removed, the cells were washed twice with DMEM. D-PBS (–) (Nacalai Tesque, Kyoto, Japan) was added to each well, and the absorbance at the measurement wavelength (excitation: 490 nm, emission: 510 nm) was measured using an absorptiometer. This experiment was performed four times.

2. Measurement of cell viability

The MTT method, which measures the viability of cultured cells by colorimetry, was used to determine enzyme activity by reducing MTT (3-(4,5-di-methylthiazol-2-yl)-2,5-diphenyltetrazolium bromide) to formazan dye. In both cell types, the number of cells was adjusted to 1.0×10^5 cells/mL, and the cells were seeded in a 96-well-multiplate and subjected to 24 h static culture in a CO_2 incubator. MTT (Dojindo Laboratories) was dissolved in D-PBS to reach a concentration of 0.5 mg/mL; this MTT solution was aliquoted at 100 μL /well in the 96-well-multiplate and cultured in a CO_2 incubator. The test solution was discarded, the formazan dye was eluted with an acidic isopropanol solution, and the absorbance at 570 nm was measured using an absorptiometer. The calculated value of each sample was divided by the value of the control group and presented as a percentage. This experiment was performed four times.

3. Observation of phagocytosis of powder particles

An autoclaved cover glass was broken and placed in a 35-mm cell culture dish. 3T3 cells and FRSK cells adjusted to 1.0×10^4 cells/mL were seeded in an individual dish and subjected to 24 h static culture in a CO_2 incubator. The adhesion and extension of the cells on the glass were confirmed using an inverted phase-contrast microscope. After removal of the culture fluid, each test solution was added, and the cells were subjected to static culture for another 24 h. The test solution was discarded, the dish bottom surface was washed with D-PBS (–) warmed to 37°C, and the cells were fixed with 2% glutaraldehyde solution warmed to 37°C for 1 h. Furthermore, the cells were washed twice with D-PBS (–) and dehydrated with 50–100% ascending series of ethanol. The solution was replaced with isoamyl acetate solution, and the cells were dried on glass using a critical point dryer (HCP-1, Hitachi, Tokyo, Japan). The sample was fixed with carbon tape, and the morphology of the two cell types was observed by SEM.

4. Annexin V-FITC/PI-stained fluorescence-activated cell sorter (FACS)

3T3 and FRSK cells were harvested by trypsin treatment, washed twice with D-PBS, and centrifuged at 1,500 rpm for 3 min. The supernatant was discarded, and the pellet was suspended in 10-fold diluted binding buffer at a density of 1.0×10^5 to 1.0×10^6 cells/mL. The sample solution (100 μL) was transferred to a culture tube and incubated with 5 μL of FITC-bound Annexin V (Nacalai Tesque) and 5 μL of PI (Nacalai Tesque) for 15 min at room temperature in the dark. To each sample tube, 400 μL of 10-fold diluted binding buffer was added and analyzed by FACS (FACS Verse, Becton Dickinson, Franklin Lakes, NJ, USA) using Cell Quest Research Software (Becton Dickinson).

5. Hematoxylin and eosin (HE) staining

3T3 and FRSK cells were seeded on sterile cover glasses and incubated in a CO_2 incubator for 24 h. The culture medium and test solution were exchanged and incubated for another 24 h. HE staining was performed according to the conventional methods. Samples were fixed with 4% paraformaldehyde (Nacalai Tesque) for 30 min. After rinsing with water, the samples were treated with Meyer hematoxylin (3000-2, Muto Pure Chemicals, Tokyo, Japan) for 20 min, fractionally washed with 1% hydrochloric acid alcohol, and washed with 1% eosin Y solution (Muto Pure Chemicals) for 10 min. They were subsequently treated with an ascending series of 60% alcohol and sealed with glycerin (Nacalai Tesque). An upright microscope was used for observation (Eclipse Ci POL, Nikon, Tokyo, Japan).

Statistical analysis

The mean and standard deviation of the acquired values were determined, and one-way analysis of variance, subset comparison (Scheffe's F method), and multiple comparisons (Bonferroni method) were performed accordingly.

RESULTS

Analysis of powder samples

1. Analysis of resin materials for CAD/CAM crowns by FT-IR

The results of the monomer content analysis by FT-IR are shown in Fig. 2. The band shape ($3,450\text{--}3,350\text{ cm}^{-1}$) was assigned to the N-H group due to the presence of UDMA. The sharp peak at $1,750\text{--}1,650\text{ cm}^{-1}$ was due to the coupling of the stretching vibration of the C-O group with the amide peak of UDMA. The band shape ($1,700$ and $1,100\text{ cm}^{-1}$) due to ester bonding was observed in TEGDMA. No significant difference was noted among the three types of resin materials in UDMA or TEGDMA in the powder cut out after polymerization.

2. Particle size distribution

No large difference was noted in the granularity distribution of the powder among the three types of resin materials and the two types of ceramic materials. The particle size of the powders was widely distributed

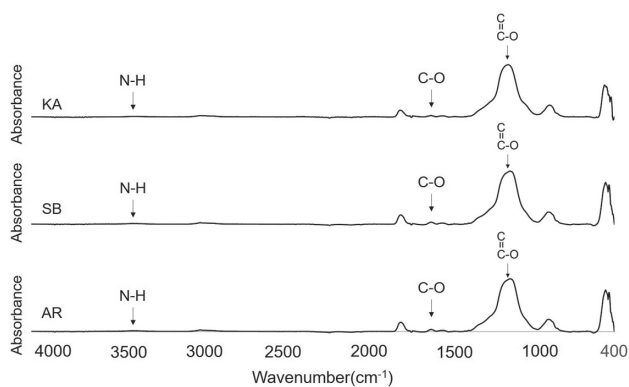


Fig. 2 The FT-IR spectrums were scanned 16 times with a resolution of 4 cm^{-1} .

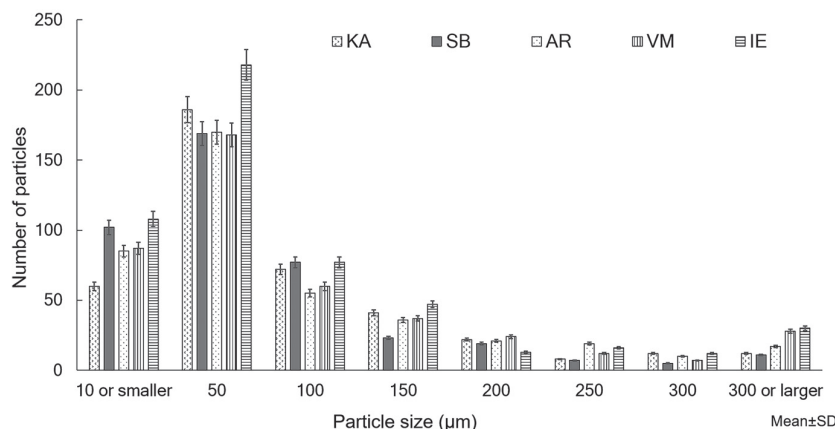


Fig. 3 Particle size distribution of particles after fine grinding of resin and ceramic blocks.

The number of particles in the field of view was repeatedly counted to be between 420 and 500.

from $10\text{ }\mu\text{m}$ to $300\text{ }\mu\text{m}$ or larger. Particles with a size of $50\text{ }\mu\text{m}$ or smaller accounted for 59–65% and $10\text{ }\mu\text{m}$ or smaller accounted for 14–24%. The rate of particles with sizes ranging from 10 to $50\text{ }\mu\text{m}$ was the highest (Fig. 3).

Measurement of oxidative stress by ROS

The results of the 3T3 cells are shown in Fig. 4a. The resin material was used as one group, and the ceramic material was used as another group for subset comparison. There was almost no difference of ROS between the resin and the ceramic materials. From the multiple comparison test, a difference was noted among the three particle sizes. The ROS value was small in the $40\text{ }\mu\text{m}$ or larger group; however, almost no difference was noted between the $5\text{--}40\text{ }\mu\text{m}$ and $5\text{ }\mu\text{m}$ or smaller groups. Almost no difference was noted among the three products of resin material; however, in the ceramic materials, a significant difference was noted in IE compared to that in VM. The results for FRSK cells are shown in Fig. 4b. Similarly, the resin material was used as one group, and ceramic material was used as another group for subset comparison. No significant differences were noted between the resin and ceramic materials. From the multiple comparison test, the influence of particle size was small compared to that of the 3T3 cells. No significant differences were noted among the products of the resin and ceramic materials.

Measurement of cell viability

The results for 3T3 cell viability are shown in Fig. 5a. As seen in the ROS test, from the subset comparison, the cell viability for resin materials was statistically significantly lower than that for ceramic materials. From multiple comparison tests with particle shape and material as design factors, among the three types of resin material, the cell viability was the lowest in SB, and it increased in the order of AR and KA. Cell viability tended to be low in the resin materials compared to that

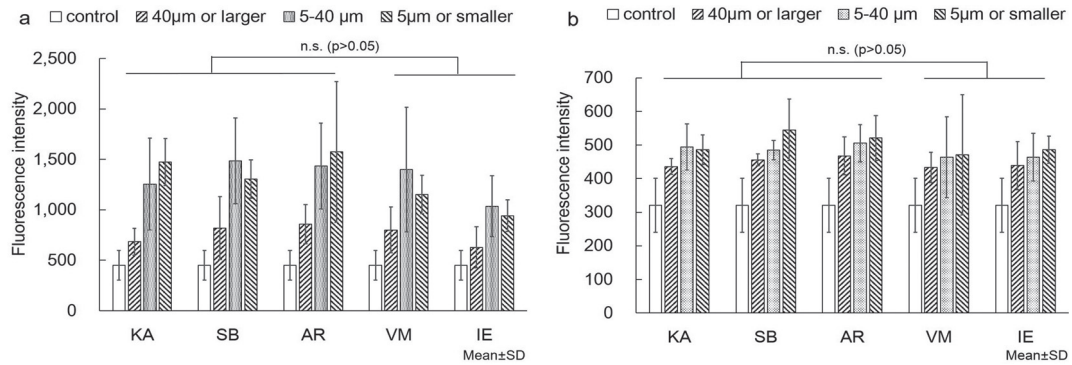


Fig. 4 Effects of resin and ceramic materials on cells by ROS assays was used to detect mitochondrial reactive oxygen species, especially superoxides. Cells exposed only to culture medium were used as negative control. A group set comparison of resin and ceramic materials was performed. a: 3T3 cells, b: FRSK cells

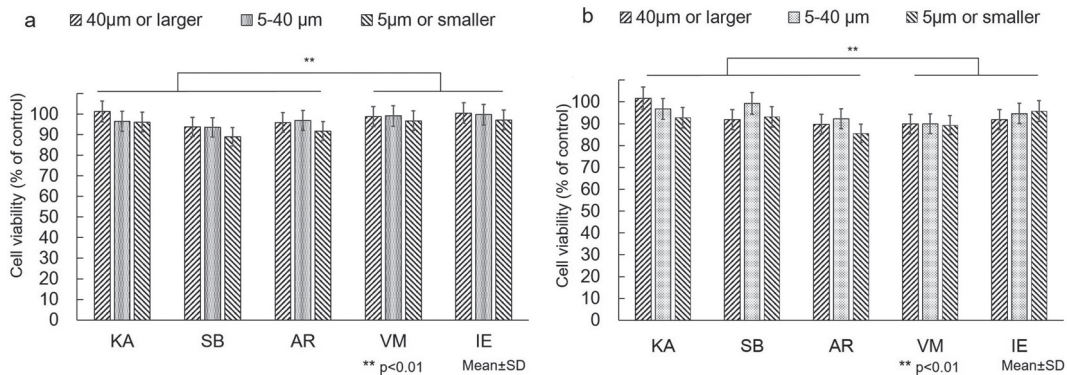


Fig. 5 Cell viability was determined by the MTT assay to identify the effects of resin and ceramic materials on cells. The group without sample was used as a negative control, and the cell viability was set at 100%. A group set comparison of resin and ceramic materials was performed. a: 3T3 cells, b: FRSK cells

in the two types of ceramic materials. There was no large difference between VM and IE. Cell viability was lower in the resin than in the ceramic materials, and the difference was significant. Among the particle sizes, cell viability tended to be high when the particle size was 40 μm or larger for both resin and ceramic materials. In the 5 μm or smaller group, cell viability tended to be low.

The FRSK cell viability results are shown in Fig. 5b. Likewise, in the subset comparison, the cell viability was statistically lower in resin material than in ceramic material. In a multiple comparison test in the same way as for 3T3 cells, in the resin materials, cell viability was the smallest in AR as observed in the 3T3 cells. In ceramic materials, the value was lower in VM than in IE. Among the particle sizes, a tendency of decrease with a decrease in the particle size observed in the 3T3 cells was noted only in the resin, KA. In the other products, particle size and cell viability varied widely among the products.

Observation of phagocytosis of fine powder particles

The SEM images are shown in Figs. 6a–f, 7a–f, 8a–f, 9a–f. Incorporation of multiple 5 μm or smaller particles into the 3T3 cells was confirmed in both resin and ceramic materials. On the other hand, in the FRSK cells, incorporation of multiple particles of the 5–40 μm group was frequently observed in both resin and ceramic materials.

Annexin V-FITC/PI FACS staining

The percentages of apoptosis, necrosis, and cell viability determined by FACS are shown in Fig. 10 and Tables 2, 3. Compared to the control group, the percentage of apoptosis increased in 3T3 cells with 5 μm or smaller KA, with 40 μm or larger SB, 40 μm or larger AR, and with 5 μm or smaller VB and IE. Necrosis increased in all groups except for <5 μm IE in 3T3 cells; in FRSK cells, it increased in all groups in KA, smaller than 5 μm of SB, 5–40 μm of AR, and with 5 μm or smaller IE, but it was lower than that in the control group in other groups. Cell viability decreased in 3T3 cells compared to that

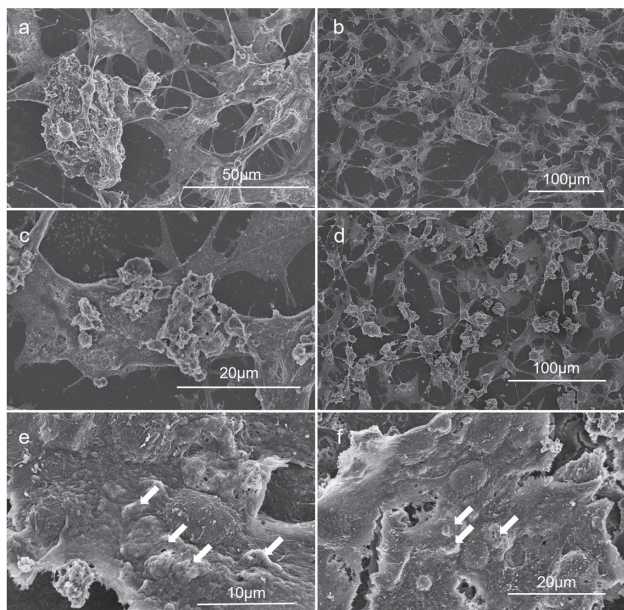


Fig. 6 a–f: SEM images of 3T3 cells with the resin particles incorporated. The white arrows indicate the unevenness of the cytoplasm due to the incorporation of resin particles smaller than 5 μm into the cell. a, b: 40 μm or larger; c, d: 5–40 μm ; e, f: 5 μm or smaller

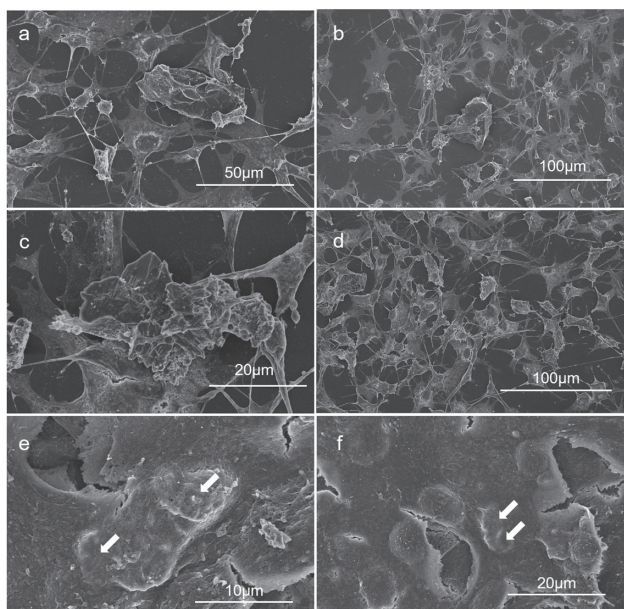


Fig. 7 a–f: SEM images of 3T3 cells with the ceramic particles incorporated. The white arrows indicate that ceramic particles of less than 5 μm are taken into the cell and these pressurize the nucleus. a, b: 40 μm or larger; c, d: 5–40 μm ; e, f: 5 μm or smaller

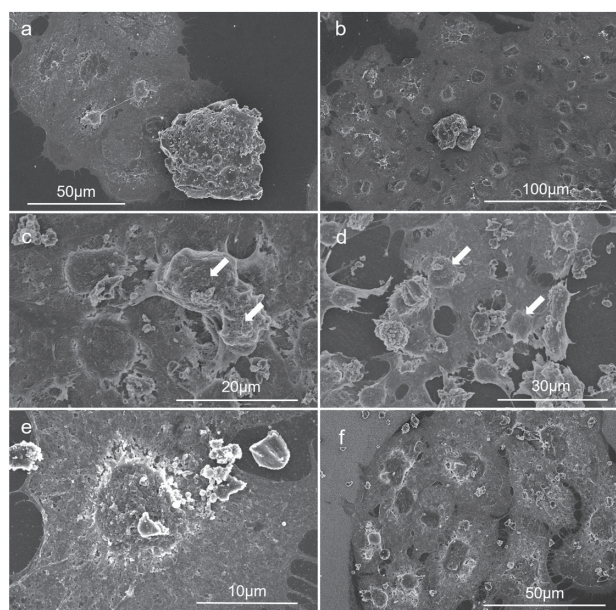


Fig. 8 a–f: SEM images of FRSK cells with particles incorporated. White arrows indicate the uptake of 5–40 μm resin particles into the cell and the deformation of the cell. a, b: 40 μm or larger; c, d: 5–40 μm ; e, f: 5 μm or smaller

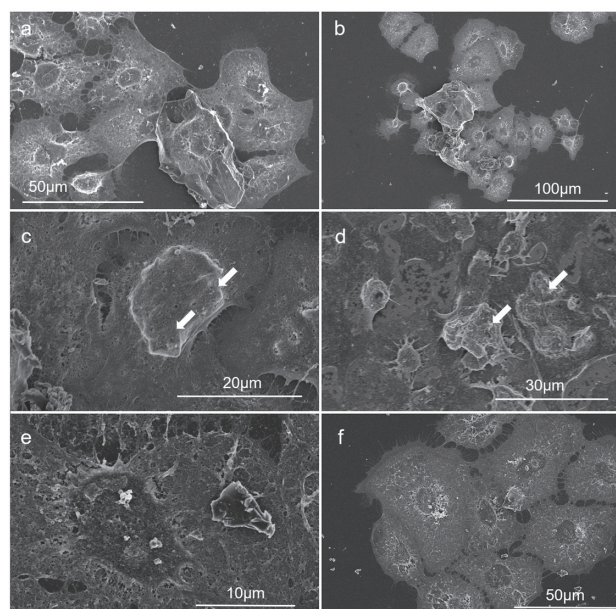


Fig. 9 a–f: SEM images of FRSK cells with particles incorporated. The white arrows show the deformation of the nucleus due to the pressure of the 5–40 μm ceramic particles. a, b: 40 μm or larger; c, d: 5–40 μm ; e, f: 5 μm or smaller

in the no-addition group, except for those with an IE 5 μm or smaller; in FRSK cells, it decreased in all groups

except for those with a VB 40 μm or larger.

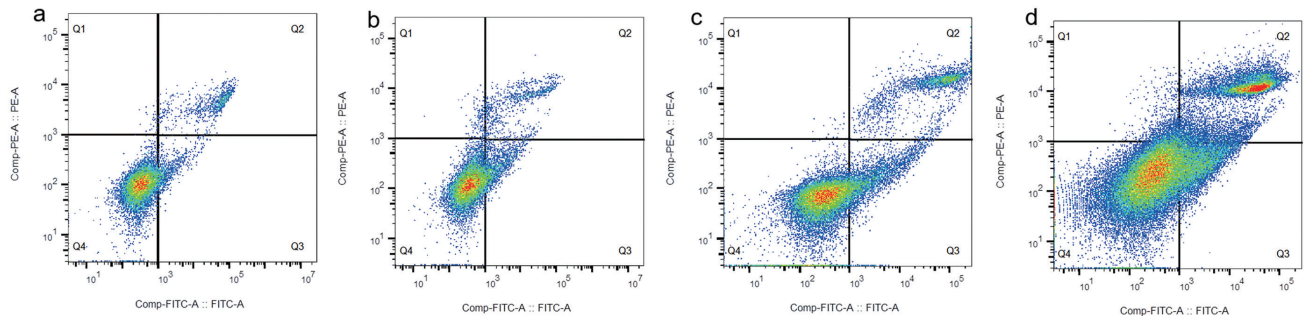


Fig. 10 a–d: Induction of apoptosis and necrosis in 3T3 cells and FRSK cells cultures by different materials after 24 h. FACS analysis after staining with annexin V/PI. Three distinct cell distribution patterns are visible: normal viable cells (lower left quadrant); apoptotic cells (lower right quadrant); necrotic and/or ‘apoptotic necrotic’ cells (upper right quadrant). a: non-treated 3T3 cells (negative controls), b: 3T3 cells with the 5 μm or smaller SB particles, c: non-treated FRSK cells (negative controls), d: FRSK cells with the 5–40 μm AR particle, a–d show the diagrams of one representative experiment. b, d reveal an increase in the proportion of apoptotic and necrotic cells.

Table 2 Induction of apoptosis and necrosis in 3T3 cells cultured with different materials after 24 h. FACS analysis after staining with annexin V-FITC/PI. Percentage of viable, apoptotic, and apoptotic necrotic/necrotic cells after a 24 h treatment with materials

		Apoptosis ratio (%)		
Materials	Size	40 μm or larger	5–40 μm	5 μm or smaller
KA		7.36±1.76	7.35±0.75	5.82±1.21
SB		5.37±1.30	7.59±0.88	6.25±1.14
AR		5.37±5.11	6.41±1.19	8.41±0.33
VM		10.94±2.43	6.44±0.50	5.99±6.87
IE		8.25±4.72	9.16±2.64	4.70±4.99
Control			6.13±4.60	
		Necrosis ratio (%)		
Materials	Size	40 μm or larger	5–40 μm	5 μm or smaller
KA		16.93±2.08	26.70±0.62	17.87±1.44
SB		9.12±1.87	18.90±0.66	22.07±0.42
AR		9.12±0.59	11.83±0.21	24.20±0.53
VM		8.10±2.76	8.43±0.57	7.96±6.72
IE		11.35±4.25	12.87±2.38	4.78±3.70
Control			6.16±5.36	
		Cell viability (%)		
Materials	Size	40 μm or larger	5–40 μm	5 μm or smaller
KA		69.43±0.25	60.33±0.15	74.43±0.20
SB		81.77±1.72	68.67±0.47	68.73±0.48
AR		81.77±2.91	80.23±0.78	63.83±0.27
VM		78.70±0.20	82.33±0.22	83.10±0.48
IE		79.43±0.42	75.43±0.22	89.40±1.11
Control			87.23±0.25	

HE staining

HE staining images in the group without the sample

and in the group with each sample are shown in Figs. 11, 12. The sample resulted in nuclear staining, nuclear

Table 3 Induction of apoptosis and necrosis in FRSK cells cultured with different materials after 24 h. FACS analysis after staining with annexin V-FITC/PI. Percentage of viable, apoptotic, and apoptotic necrotic/necrotic cells after a 24 h treatment with materials

		Apoptosis ratio (%)		
Materials	Size	40 μm or larger	5–40 μm	5 μm or smaller
KA		22.53±5.54	22.47±1.03	18.37±0.37
SB		26.90±3.96	12.21±20.19	18.73±3.44
AR		26.27±4.96	34.37±8.06	16.80±2.59
VM		10.20±0.39	17.37±0.76	14.10±1.85
IE		26.70±5.37	25.10±1.48	16.07±1.37
Control			9.01±6.21	

		Necrosis ratio (%)		
Materials	Size	40 μm or larger	5–40 μm	5 μm or smaller
KA		14.80±1.76	19.93±0.86	20.23±0.33
SB		5.97±4.13	6.74±5.26	15.80±3.66
AR		12.25±3.04	25.40±6.53	14.80±1.85
VM		7.79±0.98	9.58±0.41	9.88±0.78
IE		5.48±3.30	7.54±0.74	9.35±1.68
Control			12.37±8.97	

		Cell viability (%)		
Materials	Size	40 μm or larger	5–40 μm	5 μm or smaller
KA		61.37±4.96	54.47±0.33	59.80±0.54
SB		60.20±5.31	68.13±5.21	63.90±0.89
AR		60.07±6.56	36.90±2.35	67.07±0.61
VM		81.30±0.59	72.50±0.38	75.83±2.38
IE		67.33±1.94	66.37±0.74	74.23±1.02
Control			78.47±3.58	

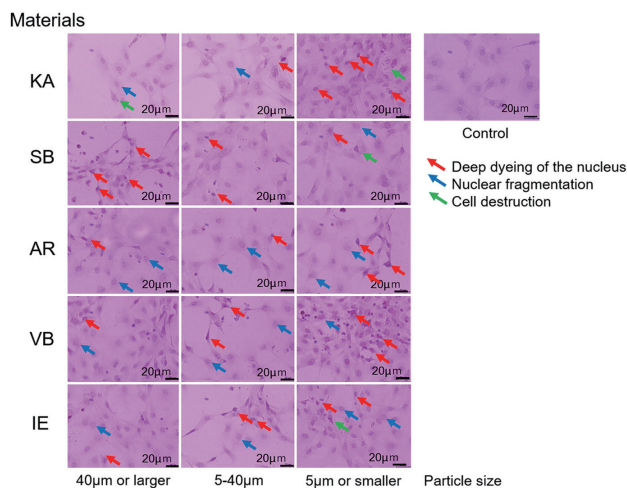


Fig. 11 3T3 cells culture with ceramic and resin materials after 24 h. HE staining of cells.

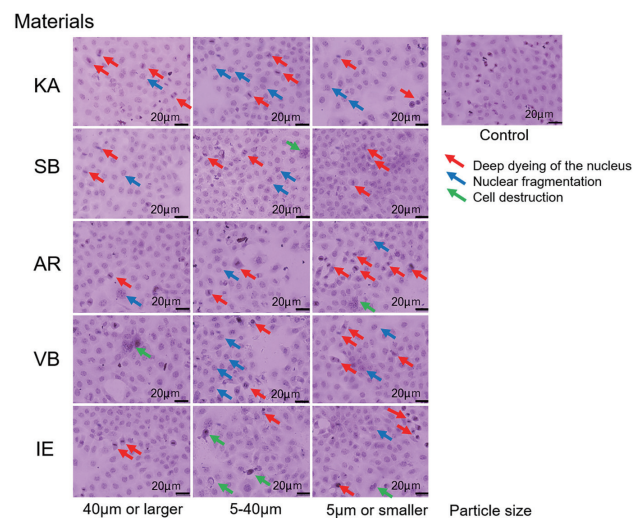


Fig. 12 FRSK cells culture with ceramic and resin materials after 24 h. HE staining of cells.

expansion, and nuclear fragmentation, which are indicators of apoptosis. In addition, destroyed cells were also observed.

DISCUSSION

On comparison between the resin materials and ceramic materials, the measurement results of oxidative stress by ROS were found to be slightly higher in the resin than in ceramic materials, and the tendency was similar between the two cell types. However, a difference was noted in the results of cell viability between the connective tissue-derived 3T3 cells and epithelium-derived FRSK cells. In the 3T3 cells, there was a slight decrease in the resin materials compared to that in the ceramic materials. In FRSK cells, the cell viability was lower in the ceramic material, VM.

Regarding the influence of particle size, generally, the surface area per volume increases as the particle size decreases, with which various biological influences on the cells may increase. In the results of ROS-based measurement, the value was clearly higher in the 5 μm or smaller group than in the 5–40 μm and 40 μm or larger groups in the 3T3 cells in all products. In the FRSK cells, the variation was large among the particle size groups, as observed in the 3T3 cells. Incorporation of 5 μm or smaller particles into the 3T3 cells was frequently observed during the observation of phagocytosis of fine powder particles by SEM. Similarly, the incorporation of 5–40- μm particles was frequently observed in FRSK cells. From the MTT and ROS tests, it was predicted that the sample caused oxidative stress and cell death.

Necrosis occurs when cells are exposed to the materials. This occurs through the collapse of the cell membrane, after which its contents flow out, and pro-inflammatory factors such as digestive enzymes and cytokines have a serious effect on the surrounding cells. However, it has been reported that fine particles, such as nanomaterials, cause apoptosis, also known as programmed cell death. Apoptosis is caused by various factors, such as particle size, shape, and surface properties^{27–29}. It is known that apoptosis is different from necrosis and it does not cause severe inflammation. Therefore, it is important to investigate the apoptosis and necrosis caused by fine dust grinding. The results of FACS suggested that there was more necrosis than apoptosis in 3T3 cells and increased apoptosis in FRSK cells. There are several possible causes of cell damage. In this experiment, it was difficult to observe a strong correlation between the results of ROS, cell viability, and cell phagocytosis; therefore, it is necessary to examine cell damage from multiple perspectives.

The three types of resin material tested in this study were resin/ceramic hybrids, and ceramics accounted for a large part of the composition, however it was possible that UDMA and TEGDMA contained in the resin materials, in which cytotoxicity decreased when these were polymerized, remained as a residual monomers with high cytotoxicity even though their amount was very small². Moreover, although it could not be clarified which

of the ceramic and resin materials were phagocytosed by cells at a higher rate, it is estimated that the angle of contact with water is larger in resin than in ceramic materials, and a large uptake of oily materials into cells has been noted. However, the involvement of multiple factors, such as particle size, wettability, hydrophobicity of the surface, and surface area, in phagocytosis has been reported. Therefore, no final judgment of whether phagocytosis had an influence could be made based on the results of this study^{26,30}.

Regarding the mechanism of manifestation of toxicity of nano- and submicron-size materials, in addition to the direct action of chemical substances eluted from these materials on the cell membrane, the presence of a system actively incorporating these materials through phagocytosis by cells is known^{26,31}. In the *in vitro* cytotoxicity test, although it depends on the test method, the cytotoxicity of materials insoluble in culture fluid is likely to be very low or lower than the detection limit^{22,31–33}. Regarding the toxicity of insoluble particles, an association with particle size has been reported in literature. Matsuoka *et al.* exposed 11 types of 0.0024–92 μm polystyrene particles to Chinese hamster-derived CHL cells for 7 days and observed the cells by SEM. They observed that particles with a particle size of 0.92–4.45 μm were likely to be phagocytosed by cells, and the cytotoxicity and abnormal chromosome inducibility were high³⁴. In our study, unlike polystyrene, which is spherical and has less surface roughness, surface unevenness was large on SEM observation and the cell type was slightly different, suggesting that the incorporated particle size was different.

The samples were vigorously stirred using a desktop vibrator; however, the possibility that the particles were not completely isolated cannot be ruled out. The isolation of nanoparticles is a major issue in nanomaterial research. The particle size of the samples in this study was larger than the submicron level, so that the particles separated through the cell strainers may have been mostly isolated by SEM observation. However, when the particle size is 5 μm or smaller, isolation by physical vibration alone may have been difficult, aggregates may have been slightly mixed, and this may have been the cause of the absence of a clear correlation between the particle size and the results of the MTT method.

Powders of resin materials and ceramic materials for commercial CAD/CAM crowns were prepared by grinding the material in a block shape using a diamond disc for dental use. However, mixing with the ingredients of the diamond disc, that is, particles of the diamond wheel and plating materials, such as nickel, needs to be considered³⁵. In this study, a new diamond disc was used, which was prepared in an attempt to avoid contamination with foreign substances as much as possible, and the samples were sufficiently washed with running water. The ingredients of grinding/abrasive materials, such as discs and points, may be mixed in the dust in clinical practice.

In actual dental practice, in addition to the materials used in this study, complex particles, such as metals,

composite resin, plaster, impression materials, and cut tooth fragments scatter in the dental treatment room³⁶⁻³⁸. Moreover, the generation of fine powder containing nano- and submicron-sized particles during grinding and cutting presents a problem; it can be performed outside the oral cavity. However, we believe that in clinical practice, the cutting method is often not considered. The size of the particles generated makes it difficult for the dentist to control the particle size during cutting and grinding, and avoiding taking up the generated dust into the body using an extraoral vacuum and dust-proof mask has become an important research subject³⁹⁻⁴¹. The particle size of the scattering dust was smaller when scattering and falling dust were compared after dust generation. It had also been reported that the rate of 10 µm or smaller particles increased as the distance between the positions of dust generation and collection increased, and 20 µm or larger dust floated in space as the distance decreased^{12,42,43}. Furthermore, in this study, most particles that were created by wear after abrasion were less than 5 µm in size, and there was no need to verify the differences between the particles. However, the smallest particle fraction produced in this experiment, less than 5 µm in size, is considered to contain nano- and submicron particles that are thought to be generated by wear.

The influence of dust produced during dental practice on health is a concern. There have been many reports on the shape, character, and influence on the body of dust^{44,45}. Regarding the specific gravity of resin materials and ceramic materials, since the specific gravity of ceramic materials is higher than that of resin materials, resin materials may be more likely to stay in the air since their specific gravity is low and the particle size is small, predicting that materials staying in the air longer are more frequently exposed to the body.

In this study, the cytotoxicity level of resin materials with a small particle size increased slightly. It was thus clarified that it is necessary to pay close attention when fine powder of resin materials is produced in dental practice.

CONCLUSIONS

Ground fragments of three types of resin materials and two types of ceramic materials for CAD/CAM crowns were separated into three particle sizes (40 µm or larger, 5–40 µm, 5 µm or smaller), and oxidative stress by ROS, cell viability, and FACS of 3T3 cells and FRSK cells exposed to the particles were measured accordingly. The influence of the resin materials on the cells tended to be slightly larger than that of the ceramic materials, whereas the relationship with the particle size was different between the two cell types. In addition, phagocytosis of powder particles was observed by SEM, and incorporation of particles smaller than 5 µm was confirmed in 3T3 cells. In FRSK cells, incorporation of 5–40-µm particles into the cells was frequently observed, suggesting that the particle size of easily incorporated dust is different depending on the cell type. In addition,

HE staining showed histological images of nuclear and cellular damage caused by the addition of the sample. In this study, the effects of CAD/CAM materials in the form of fine powder on cells were examined using basic data on biological safety, and it was found that cellular damage appeared differently depending on the size of the particles and the type of cells.

ACKNOWLEDGMENTS

The author would like to thank the members of the Department of Biomaterials and Institute of Dental Research, Osaka Dental University. The author would like to grateful to Dr. Tsumano N, Dr. Akimoto H, and Ph.D. Iwasaki K for their technical support of tissue culture and FACS.

REFERENCES

- 1) Sannino G, Germano F, Arcuri L, Bigelli E, Arcuri C, Barlattani A. CEREC CAD/CAM chairside system. *Oral Implantol (Rome)* 2015; 3: 57-70.
- 2) Engler MLPD, Güth JF, Keul C, Erdelt K, Edelhoff D, Liebermann A. Residual monomer elution from different conventional and CAD/CAM dental polymers during artificial aging. *Clin Oral Investig* 2020; 24: 277-284.
- 3) Hynková K, Voborná I, Linke B, Levin L. Compendium of current ceramic materials used for the CAD/CAM dentistry. *Acta Stomatol Marisiensis J* 2021; 4: 7-17.
- 4) Lauvahutanon S, Hidekazu T, Shiozawa M, Iwasaki N, Asakawa Y, Oki M, *et al.* Mechanical properties of composite resin blocks for CAD/CAM. *Dent Mater J* 2014; 33: 705-710.
- 5) Ludovichetti FS, Trindade FZ, Werner A, Kleverlaan CJ, Fonseca RG. Wear resistance and abrasiveness of CAD-CAM monolithic materials. *J Prosthet Dent* 2018; 120: 318.e1-318.e8.
- 6) Furtado de Mendonca A, Shahmoradi M, Gouvêa CVD, de Souza GM, Ellakwa A. Microstructural and mechanical characterization of CAD/CAM materials for monolithic dental restorations. *J Prosthodont* 2019; 28: e587-594.
- 7) Sonmez N, Gultekin P, Turp V, Akgungor G, Sen D, Mijiritsky E. Evaluation of five CAD/CAM materials by microstructural characterization and mechanical tests: A comparative in vitro study. *BMC Oral Health* 2018; 18: 5.
- 8) Tamim H, Skjerven H, Ekfeldt A, Rønold HJ. Clinical evaluation of CAD/CAM metal-ceramic posterior crowns fabricated from intraoral digital impressions. *Int J Prosthodont* 2014; 27: 331-337.
- 9) Batson ER, Cooper LF, Duqum I, Mendonça G. Clinical outcomes of three different crown systems with CAD/CAM technology. *J Prosthet Dent* 2014; 112: 770-777.
- 10) Wang W, Li T, Luo X, Zhang K, Cao N, Liu K, *et al.* Cytotoxic effects of dental prosthesis grinding dust on RAW264.7 cells. *Sci Rep* 2020; 10: 14364.
- 11) Cokic SM, Ghosh M, Hoet P, Godderis L, Van Meerbeek B, Van Landuyt KL. Cytotoxic and genotoxic potential of respirable fraction of composite dust on human bronchial cells. *Dent Mater* 2020; 36: 270-283.
- 12) Johnston NJ, Price R, Day C, Sandy JR, Ireland AJ. Quantitative and qualitative analysis of particulate production during simulated clinical orthodontic debonds. *Dent Mater* 2009; 25: 1155-1162.
- 13) Van Landuyt KL, Yoshihara K, Geebelen B, Peumans M, Godderis L, Hoet P, *et al.* Should we be concerned about composite (nano-)dust? *Dent Mater* 2012; 28: 1162-1170.
- 14) Choudat D, Triem S, Weill B, Vicrey C, Ameille J, Brochard

- P, *et al.* Respiratory symptoms, lung function, and pneumoconiosis among self employed dental technicians. *Br J Ind Med* 1993; 50: 443-449.
- 15) Zenthöfer A, Rammelsberg P, Schmitt C, Ohlmann B. Wear of metal-free resin composite crowns after three years in service. *Dent Mater J* 2013; 32: 787-792.
 - 16) Vanoorbeek S, Vandamme K, Lijnen I, Naert I. Single-tooth restorations: A 3-year clinical study. *Int J Prosthodont* 2010; 23: 223-231.
 - 17) Yesil ZD, Alapati S, Johnston W, Seghi RR. Evaluation of the wear resistance of new nanocomposite resin restorative materials. *J Prosthet Dent* 2008; 99: 435-443.
 - 18) Rizo-Gorrita M, Herráez-Galindo C, Torres-Lagares D, Serrera-Figallo MÁ, Gutiérrez-Pérez JL. Biocompatibility of polymer and ceramic CAD/CAM materials with human gingival fibroblasts (HGFs). *Polymers (Basel)* 2019; 11: 1446.
 - 19) Campaner M, Takamiya AS, Bitencourt SB, Mazza LC, de Oliveira SHP, Shibayama R, *et al.* Cytotoxicity and inflammatory response of different types of provisional restorative materials. *Arch Oral Biol* 2020; 111: 104643.
 - 20) Alamoush RA, Kushnerev E, Yates JM, Satterthwaite JD, Silikas N. Response of two gingival cell lines to CAD/CAM composite blocks. *Dent Mater* 2020; 36: 1214-1225.
 - 21) Manshian BB, Himmelreich U, Soenen SJ. Standard cellular testing conditions generate an exaggerated nanoparticle cytotoxicity profile. *Chem Res Toxicol* 2017; 30: 595-603.
 - 22) Nativo P, Prior IA, Brust M. Uptake and intracellular fate of surface-modified gold nanoparticles. *ACS Nano* 2008; 2: 1639-1644.
 - 23) Mahmood M, Casciano DA, Mocan T, Iancu C, Xu Y, Mocan L, *et al.* Cytotoxicity and biological effects of functional nanomaterials delivered to various cell lines. *J Appl Toxicol* 2010; 30: 74-83.
 - 24) Kroll A, Dierker C, Rommel C, Hahn D, Wohlleben W, Schulze-Isfort C, *et al.* Cytotoxicity screening of 23 engineered nanomaterials using a test matrix of ten cell lines and three different assays. *Part Fibre Toxicol* 2011; 8: 9.
 - 25) Sharma G, Valenta DT, Altman Y, Harvey S, Xie H, Mitragotri S, *et al.* Polymer particle shape independently influences binding and internalization by macrophages. *J Control Release* 2010; 147: 408-412.
 - 26) Champion JA, Mitragotri S. Role of target geometry in phagocytosis. *Proc Natl Acad Sci U S A* 2006; 103: 4930-4934.
 - 27) Fröhlich E, Samberger C, Kueznik T, Absenger M, Roblegg E, Zimmer A, *et al.* Cytotoxicity of nanoparticles independent from oxidative stress. *J Toxicol Sci* 2009; 34: 363-375.
 - 28) Manke A, Wang L, Rojanasakul Y. Mechanisms of nanoparticle-induced oxidative stress and toxicity. *Biomed Res Int* 2013; 2013: 942916.
 - 29) Zhao T, Tan L, Zhu X, Huang W, Wang J. Size-dependent oxidative stress effect of nano/micro-scaled polystyrene on *Karenia mikimotoi*. *Mar Pollut Bull* 2020; 154: 111074.
 - 30) Yin H, Too HP, Chow GM. The effects of particle size and surface coating on the cytotoxicity of nickel ferrite. *Biomaterials* 2005; 26: 5818-5826.
 - 31) Hattori K, Nakadate K, Morii A, Noguchi T, Ogasawara Y, Ishii K. Exposure to nano-size titanium dioxide causes oxidative damages in human mesothelial cells: The crystal form rather than size of particle contributes to cytotoxicity. *Biochem Biophys Res Commun* 2017; 492: 218-223.
 - 32) Hsu SY, Morris R, Cheng F. Signaling pathways regulated by silica nanoparticles. *Molecules* 2021; 26: 1398.
 - 33) Watari F. Risk assesment and safty measures of nanomaterials. Fumio W, editor. *frontier-books*; 2010. 96-103 p.
 - 34) Matsuoka A, Önfelt A, Matsuda Y, Isama K, Sakoda H, Kato R, *et al.* Polyploidy induction by spherical size standard polystyrene particles in a Chinese hamster cell line CHL. *Bull Natl Inst Heal Sci* 2015; 2015: 29-36.
 - 35) Corazza PH, De Castro HL, Feitosa SA, Kimpara ET, Della Bona A. Influence of CAD-CAM diamond bur deterioration on surface roughness and maximum failure load of Y-TZP-based restorations. *Am J Dent* 2015; 28: 95-99.
 - 36) Brune D, Beltesbrekke H, Strand G. Dust in dental laboratories. Part II: Measurement of particle size distributions. *J Prosthet Dent* 1980; 44: 82-87.
 - 37) Lang A, Ovsenik M, Verdenik I, Remškar M, Oblak Č. Nanoparticle concentrations and composition in a dental office and dental laboratory: A pilot study on the influence of working procedures. *J Occup Environ Hyg* 2018; 15: 441-447.
 - 38) Nilsen BW, Jensen E, Örtengren U, Bang B, Michelsen VB. Airborne exposure to gaseous and particle-associated organic substances in resin-based dental materials during restorative procedures. *Eur J Oral Sci* 2019; 127: 425-434.
 - 39) Breul S, Van Landuyt KL, Reich FX, Högg C, Hoet P, Godderis L, *et al.* Filtration efficiency of surgical and FFP3 masks against composite dust. *Eur J Oral Sci* 2020; 128: 233-240.
 - 40) Liu MH, Chen CT, Chuang LC, Lin WM, Wan GH. Removal efficiency of central vacuum system and protective masks to suspended particles from dental treatment. *PLoS One* 2019; 14: e0225644.
 - 41) Florez FLE, Thibodeau T, Oni T, Floyd E, Khajotia SS, Cai C. Size-resolved spatial distribution analysis of aerosols with or without the utilization of a novel aerosol containment device in dental settings. *Phys Fluids (1994)* 2021; 33: 085102.
 - 42) Brune D, Beltesbrekke H. Levels of airborne particles resulting from handling alginate impression material. *Scand J Dent Res* 1978; 86: 206-210.
 - 43) Brune D, Beltesbrekke H. Dust in dental laboratories. Part I: Types and levels in specific operations. *J Prosthet Dent* 1980; 43: 687-692.
 - 44) Bacchetta R, Santo N, Valenti I, Maggioni D, Longhi M, Tremolada P. Comparative toxicity of three differently shaped carbon nanomaterials on *Daphnia magna*: Does a shape effect exist? *Nanotoxicology* 2018; 12: 201-223.
 - 45) Zhao X, Ng S, Heng BC, Guo J, Ma L, Tan TTY, *et al.* Cytotoxicity of hydroxyapatite nanoparticles is shape and cell dependent. *Arch Toxicol* 2013; 87: 1037-1052.